Phase Diagram of Dense H_{2}-He Mixtures: Evidence for Strong Chemical Association, Miscibility, and Structural Change

Jinhyuk Lim and Choong-Shik Yoo

Phys. Rev. Lett. **120**, 165301 — Published 19 April 2018

DOI: 10.1103/PhysRevLett.120.165301

Phase Diagram of Dense H_2-He Mixture: Evidence for Strong Chemical Association, Miscibility and Structure Change

Jinhyuk Lim and Choong-Shik Yoo

Institute for Shock Physics and Department of Chemistry

Washington State University, Pullman, WA99164

Abstract

The phase diagram of hydrogen-helium mixture is presented to 75 GPa, underscoring the formation of metastable H_2-rich crystallite in He-rich fluid mixtures and the structural phase transition in He lattice at ~52 GPa. The Raman data also indicates a significant level of mixing between H_2 and He even in solids, giving rise to new vibrational bands in He-rich solid at ~2400 cm^{-1} for H-He stretching and 140 cm^{-1} for the lattice phonon of H_2 incorporated hcp-He. Therefore, the present result signifies unexpected, strong chemical association of the interstitial-filled guest molecules (H_2 or He) with the host lattice (*hcp*-He or H_2) in this quantum solid mixture.

Hydrogen (H_2) and helium (He) are two most fundamental solids abundant in the Universe. Compression behaviors of H_2 and He are critical to understand many body effects of these quantum solids [1,2]; develop new condensed matter theories [3-5]; and get insights into the internal structure of the Giant planets [6,7]. The equations of state (EOS) of H_2 and He, for example, provide the critical constraints for modeling the internal structure, dynamics and conductivity of the planets. Recent theories have predicted the phase separation of H_2 and He at high pressures and temperatures [8,9]. As such, it is thought that heavier He precipitating down from the upper H_2-He layer generates gravitational energy that drives planetary dynamics and contributes to the luminosity observed in Saturn [9]. The exact pressure-temperature (P-T) conditions, chemical states (i.e., liquid, solid, metallic, insulating, etc.), and properties (EOS, diffusivity, miscibility, etc.) of H_2 and He, on the other hand, provide critical constraints for the thickness and chemical composition of layer boundaries and the origin of giant magnetic fields observed in these Giant planets [10].

Recently, there has been a rapid progress in understanding the phase diagram of hydrogen at high pressures [11-15]. Several new phases including phase IV [11], V [12], and VI [13] have been suggested in the pressure regime where hydrogen is reported to become a narrow bandgap semiconductor (above 250 GPa [14]) and even a metallic solid (above 400 GPa [15]). Helium is known to stay in *hcp* phase to ~58 GPa at room temperature [16] in contrast to the theoretical prediction of *fcc* phase [17]. This makes He unique from other inert gas solids, underscoring its large anharmonicity and quantum effect [3]. On the other hand, a little is known about the binary phase diagram of H_2 and He, since the first phase diagram presented to 10 GPa four decades ago in 1973 [18] and 1987 [19]. This is despite the interesting features observed in the isothermal pressure-composition phase diagram of H_2+He, such as the presence of immiscible two-fluids

phase region and collective compression of H_2 in fluid He. Yet, no information is known about the structure and phase stability of solid H_2 and He mixtures above 12 GPa.

The considerable mobility of H_2 (or He) can contribute to its miscibility with He (or H_2) and the planetary "ices" (H_2O, NH_3 and CH_4), which can significantly affect the EOS and other properties such as the conductivity and diffusivity. The mixing of hydrogen with the planetary ices, for example, can be readily observed, when hydrogen isotope deuterium (D_2) is introduced in H_2O in the form of the proton exchange between H_2O and D_2 as evident from the Raman spectra even at 50 GPa [20]. A similar level of high mobility and miscibility is expected in He mixtures with other elemental solids [21-24]; yet, proving this conjecture in H_2+He mixtures remains extremely challenging because of the difficulty probing the presence of He in those mixtures. In this Letter, using a sensitive confocal micro-Raman system, we present the spectral evidence that there is a sufficient level of mixing in H_2+He solid mixtures, resulting in strong chemical association of H_2 in *hcp*-He lattice in He-rich solid even at pressures well below 100 GPa where H_2 and He have been considered as chemically inert [3, 25].

The present results are summarized in the binary phase diagram of H_2-He mixture (Fig. 1), consisting of homogenous H_2-He mixture F (below 5 GPa), H_2-rich fluid F_1, He-rich fluid F_2, H_2-rich solid S_1 and S_1' (appeared in fluid He + solid H_2 mixtures in the He-rich fluid), He-rich solid S_2 and S_3 (appeared above 52 GPa). This phase diagram is constructed based on the reproducible Raman data taken from a large number (twenty three) of high-pressure samples with seven different compositions (including pure H_2 and pure He). The detailed experimental method and the spectral data are presented in the Supplementary Information (Figs. S1-S17).

Figure 2 shows Raman spectra of 1:1 H_2:He mixture to 75 GPa, plotted for the high

frequency region of H_2 vibron. At 2.2 GPa H_2 and He form a homogeneous fluid mixture (F), of which H_2 vibron appears blue-shifted (4204.8 cm^{-1}) and broadened (FWHM = 26.0 cm^{-1}) compared to those of pure H_2 vibron (4183.6 cm^{-1}, FWHM = 12.0 cm^{-1}) at the same pressure (shown in the grey spectrum). Upon the solidification of H_2 between 5.1 and 6.4 GPa, the homogeneous fluid mixture separates into three distinctive regions (see the inset photo): solid H_2 (S_1), H_2-rich fluid (F_1) and He-rich fluid (F_2), which can be identified by the corresponding H_2 vibrons. The sharp H_2 vibron (4214.3 cm^{-1}, FWHM = 7.5 cm^{-1}) of S_1 (here-to-after call it as the S_1 vibron) at 6.4 GPa agrees well with that of pure solid H_2 (4211.9 cm^{-1}, FWHM = 7.1 cm^{-1}) [26]. The asymmetric tail of the S_1 vibron at 6.4 GPa is due to an incomplete phase transition of S_1 out of F_1. Interestingly, the F_1 vibron appears blue shifted (4229 cm^{-1}) and broadened (FWHM = 25.3 cm^{-1}) from the S_1, while the F_2 vibron has even stronger blue shift (4343.3 cm^{-1}) and broadness (FWHM = 66.8 cm^{-1}). The strong blue shift of the F_2 vibron is due to the larger compressibility of fluid He than solid H_2 [18,27]. Note that pure H_2 solidifies at around 5.5 GPa. Therefore, the fact that the F_1 is even present at 6.4 GPa is an indication of He inclusions disturbing the ordering of H_2 molecules. Above 6.5 GPa, the F_1 completely transforms to the S_1, of which vibron well tracks that of pure H_2. However, the F_2 vibron remains strongly blue shifted and extremely broad, until the F_2 transforms into He-rich solid S_2 at 11.9 GPa.

Upon the completion of the F_2 to S_2 transformation at 12.6 GPa, the S_2 vibron splits into two sharp peaks, arising from the interstitial filled H_2 molecules in He lattice (S_2). A small vibron overlapping with the S_1 vibron is apparently from the S_1 and S_2 boundary. The 2:1 intensity ratio of the S_2 doublet is consistent with the degeneracy ratio of tetrahedral and octahedral sites in *hcp*-He. Importantly, the S_2 doublet disappears abruptly above 52 GPa, whereas the S_1 vibron still remains strong. This result clearly indicates a structural change in H_2

incorporated *hcp*-He at 52 GPa. All spectral changes observed in the S2, including the doublets at ~ 4300 cm^{-1} and ~2400 cm^{-1}, and the low frequency phonon at ~140 cm^{-1}, occur irreversibly upon the pressure downloading from above 52 GPa. The irreversible spectral change, in turn, indicates a small energy difference between two He phases and thereby a close packed structure for the new high-pressure phase [28].

The present spectral data also reveals unexpected Raman features in a relatively low frequency region of H_2 vibron (Fig. 3), suggesting strong chemical association between H_2 and He in the S_2 phase. The S_2 peaks at ~140 cm^{-1} and ~2350 cm^{-1} (doublet) begin to appear upon the solidification at 11.9 GPa and disappear above 52 GPa, analogous to the pressure dependence of the blue-shifted S_2 vibron in Fig. 2. These new features are weak but reproducible over all concentrations and in different sample configurations (see Figs. S8-S17). Moreover, the intensity of the 2350 cm^{-1} peak increases considerably (by a factor of ten) as increasing the He concentration above 50 % (Fig. 3 inset). We attribute these peaks to a lattice phonon (E_{2g} shear mode of H_2 incorporated *hcp*-He) at ~140 cm^{-1} and a H-He vibron at 2350 cm^{-1} of the S_2. The E_{2g} phonon was observed in pure He at 20 K and 1 GPa– not at ambient temperature and higher pressures [29]. In fact, the calculated frequency of H-He stretching in linear HHeF is about 2304 cm^{-1} [30] in a good agreement with the observed frequency 2350 cm^{-1} considering the pressure difference.

The pressure-dependent Raman shifts of H_2 and He mixtures for five different concentrations are plotted in Fig. 4, together with that of pure H_2: (a) high-frequency H_2 vibron below 11.9 GPa and (b) above 11.9 GPa, and (c) low-frequency H-H/H-He vibron to 75 GPa. In homogeneous fluid mixture F, the degree of the blue shift in H_2 vibron is proportional to He concentration as observed previously [19,27]. In the 7:3, 5:5, and 3:7 mixtures, phase F separates

into two immiscible F_1 and F_2 fluids between 5 and 6.5 GPa. As mentioned, H_2 vibron in F_2 is more blue-shifted than in F_1, but the magnitude of pressure shift becomes independent of the composition. The peak position of S_1 vibron faithfully tracks that of pure H_2 to 75 GPa - the highest pressure studied 75 GPa (Fig. 4b). Above ~ 6.5 GPa the pressure shift of the S_1 vibron well tracks that in pure H_2. On the other hand, the F_2 vibron remains as a singlet to 12 GPa, then upon the solidification to the S_2 it splits into several peaks all strongly blue shifted from pure H_2 vibron. Again, these S_2 vibrons disappear abruptly at ~52 GPa. The 3:7 and 1:9 He-rich mixtures show even three blue-shifted H_2 vibrons in S_2, apparently coming from micro-crystallites (see Figs. S10 and S12) formed in He-rich area, presumably from the strong chemical associations. Especially, in 1:9 He-rich mixture a new crystallite formed in He-rich area (see the insets in Fig. 4). Note that these vibrons of the new crystal remain well beyond 52 GPa, the pressure-dependence similar to H_2-rich solid (S_1). Thus, we call it as S_1'.

The low-frequency modes (Fig. 4c) exhibit a similar pressure dependence to the high-frequency H_2 vibrons (Fig. 4b). That is, the disappearance of S_2 modes above 52 GPa. It also shows the formation of S_1' in the 1:9 mixture, which exhibits a set of new peaks at ~3000-3200 cm^{-1} – the spectral region where H-H vibrons in hydrides appear such as CsH_7 [31] and NaH_9 [32]. The inset in Fig. 4a clearly shows the coexistence of three solid phases, S_1, S_2, and S_1' in the 1:9 mixture. Note that contrary to the S_1 and S_2, the S_1' forms a crystal-like solid *only* in highly He-rich mixture of which solidification pressure rapidly increases with He concentration (see Fig. 1). Therefore, it is likely that the S_1' is a H_2-rich solid grown from fluid He.

The present results suggest the formation of strongly associate phases in both H_2-rich and He-rich solid mixtures, indicating considerable miscibility between H_2 and He at all

compositions studied (see Figs. S8-S17). This is unexpected because the previous study has reported a diminishing miscibility between solid H_2 and solid He with increasing pressure above 12 GPa [33]. Nevertheless, the formation of strongly associated phase can be understood in terms of the polarization of small amount of H_2 impurities captured in between *hcp*-He layers in He-rich solid S_2, forming a paired charge transferred He hydrides, He - $H_2^{\delta+}$ - He - $H_2^{\delta-}$ - He. A similar dipolar pairing of H_2 molecules ($H_2^{\delta+}$… $H_2^{\delta-}$) was observed in dense pure H_2 (*i.e.*, HA phase) [34]. Based on the previous single crystal X-ray data of He (a= 2.069 Å and c=3.379 Å at 17.4 GPa [35]), this model gives the interlayer H-He distance along the [100] to be ~0.85 Å, well compared with d(He-He) = 1.03 Å and d(H-H) = 0.75 Å. Then, the extended (*i.e.* charge paired H_2) nature of this model gives rise to two nearly degenerated in-phase and out-of-phase vibrational modes, as observed in Fig. 3. The intensity enhancement of the 2400 cm^{-1} bands at the higher He concentrations (Fig. 3c) reflects the greater polarizability of hydrogen, supporting the model.

In the S_1' solid, on the other hand, the polarization may occur on the interstitial filled He to form hydrogen-rich He hydrides $(H_2)_nH^{\delta-}He^{\delta+}$ (n>1). The excess H_2 molecules then help screen the hydride-hydride repulsion, as previously suggested for alkali metal hydrides [31,32]. The nature of local chemical bonding of HHeH can then be described in terms of a four-electron three-centered system (as if H_3^-), consisting of σ_g^2 bonding and σ_u^2 non-bonding in the linear configuration. As pressure increases, the linear HHeH structure starts to distort (or bend), destabilizing the nonbonding orbital more toward the σ_g* anti-bonding and eventually leading to a structural change.

The present data provides new constraints for the binary phase diagram of H_2 and He mixtures to 75 GPa as presented in Fig. 1. The present phase diagram emphasizes the formation of H_2-rich crystallite (S_1') in He-rich fluid mixtures and the structural phase transition in He lattice (from the S_2 to the S_3) at ~52 GPa. It also indicates the phase separation of homogeneous H_2+He mixture (F) into two immiscible fluids (F_1 and F_2) in the narrow pressure region between ~5.0-6.5 GPa. Clearly, the S_1' phase is metastable, formed by faster diffusion of solid H_2 crystallites in fluid He and, once it formed, exists at least to 75 GPa.

The presence of structural phase transition in He-rich lattice at 52 GPa is in contrast to the behavior of pure He, which remains in *hcp* at least to 58 GPa at ambient temperature [16]. Nevertheless, the present spectral data clearly indicates the disruption of *hcp* layers and thereby the interlayer H-He bonding. A potential structure for the new phase is obviously *fcc* – the phase exists only along the melt between 15 K and 285 K below 12 GPa in pure He. However, it is not known if the disorder introduced by adding H_2 impurities would expand the stability of *fcc* above 52 GPa at ambient temperatures [3,17]. Clearly, further structural studies are required to signify this conjecture and elucidate the role of H_2 impurities in this quantum solid H_2-He mixture at high pressures.

The present work has been done in support of the NNSA (DE-NA 0003342) and NSF-DMR (*Grant No.* 1701360), ACS-PRF (No. 54806-ND10), and the DCO-EPC through Sloan Foundation. We thank Dr. John Tse and Dr. Paul Loubeyre for valuable discussion.

REFERENCES

1. E. Babaev, A. Sudbo, and N.W. Ashcroft, *Phys. Rev. Lett.* **95**, 105301 (2005).
2. E. Kim and M.H.W. Chan, *Science* **305**, 1941 (2004).
3. J. M. McMahon, M. A. Morales, C. Pierleoni, and D. M. Ceperley, *Rev. Mod. Phys*. **84**, 1607 (2012).
4. N. W. Ashcroft, *Phys. Rev. Lett*. **92**, 187002 (2004).
5. C. J. Pickard, M. Martinez-Canales, and R.J. Needs, *Phys. Rev. B* **85**, 214115 (2012).
6. T. Guillot, *Science* **286**, 72 (1999).
7. W. B. Hubbard, A. Burrows, and J. I. Lunine, *Ann. Rev. Astron. Astrophys*. **40**, 103 (2002).
8. M. A. Morales, S. Hamel, K. Caspersen, and E. Schwegler, *Phys. Rev. B* **87**, 174105 (2013).
9. J. J. Fortney and W.B. Hubbard, *Astrophys. J.* **608**, 1039 (2004).
10. R. Holme and J. Bloxham, *J. Geophys. Res.* **101**, 2177 (1996).
11. R. T. Howie, C. I. Guilaume, T. Scheler et al., *Phys. Rev. Lett.* **108**, 125501 (2012).
12. M. I. Eremets, I. A. Troyan and A. P. Drozdov, https://arxiv.org/abs/1601.04479 (2016).
13. R. P. Dias, O. Noked, and I. F. Silvera, *Phys. Rev. Lett.* **116**, 145501 (2016).
14. M. I. Eremets and I. A. Troyan, *Nat. Mat.* **84**, 927 (2011).
15. R. P. Dias and I. F. Silvera, *Science* **335**, 715 (2017).
16. P. Loubeyre, R. LeToullec, and J. P. Pinceaux, *Phys. Rev. Lett*. **71**, 2272 (1993).
17. J. P. Franck and W. B. Daniels, *Phys. Rev. Lett.* **44**, 259 (1980)
18. W. B. Streett, *Astrophys. J.* **186**, 1107 (1973).
19. P. Loubeyre, R. Le Toullec, and J.P. Pinceaus, *Phys. Rev. B* **36**, 3723 (1987).
20. G. Borstad and C.S. Yoo, *J. Chem. Phys.* **135**, 174508 (2011).

21. X. Dong, A. R. Oganov, A. F. Goncharov, et al., *Nat. Chem.* **9**, 440 (2017).

22. M. Somayazulu, P. Dera, A. F. Goncharov, S. A. Gramsch, et al., *Nat. Chem.* **2**, 50 (2010).

23. B. W. Bakr, D. G. A. Smith, and K. Patkowski, J. Chem. Phys. 139, 144305 (2013).

24. C. Ji, A. F. Goncharov, V. Shukla, N. K. Jena, et al. *Proc. Nat. Acad. Sci*. **114**, 3596 (2017).

25. P. Loubeyre, R. LeToullec, D. Hausermann, et al., *Nature* **383**, 702 (1996).

26. R. T. Howie, P. Dalladay-Simpson, and E. Gregoryanz, *Nat. Mater*. **14**, 495 (2015).

27. P. Loubeyre, R. Le Toullec, and J. P. Pinceaux, *Phys. Rev. B* **32**, 7611 (1985).

28. H. Cynn, C. S. Yoo, B. Baer, et al., *Phys. Rev. Lett.* **86**, 4552 (2001).

29. G. H. Watson and W. B. Daniels, *Phys. Rev. B* 31, 4705 (1985).

30. M. W. Wong, *J. Am. Chem. Soc*. **122**, 6289 (2000).

31. A. Shamp, J. Hooper, and E. Zurek, *Inorg. Chem.* **51**, 9333 (2012).

32. P. Baettig and E. Zurek, *Phys. Rev. Lett*. **106**, 237002 (2011).

33. P. Loubeyre, R. Le Toullec, and J. P. Pinceaux, *J. Phys. Condens. Matter* **3**, 3183 (1991).

34. R. J. Hemley, Z. G. Soos, M. Hanfland, and H.-K. Mao, *Nature* **369**, 384 (1994).

35. H. K. Mao, R. J . Hemley, Y. Wu, et al., *Phys. Rev. Lett*. **60**, 2649 (1988).

36. See Supplementary Materials [url] for the detailed experimental data as obtained in this work, which includes seventeen figures (Figs. S1 to S17), corresponding captions, and Refs. [37-43].

37. H. K. Mao, J. Xu, and P. M. Bell, *J. Geophys. Res*. **91**, 4673 (1986).

38. J. Lim and C. S. Yoo, *Appl. Phys. Lett.* **109**, 1 (2016).

39. Y. J. Ryu, M. Kim, and C.-S. Yoo, *Sci. Rep*. **5**, 1 (2015).

40. Y. Akahama and H. Kawamura, *J. Appl. Phys.* **100**, 044516 (2006).

41. H. Schneider, W. Häfner, and A. Wokaun, *J. Chem. Phys.* **96**, 8046 (1992).

42. W. L. Vos *et al*., *Nature* **358**, 46 (1992).

43. H. Olijnyk and A. P. Jephcoat, *J. Phys.: Condens. Matter* **9**, 11219 (1997).

Figure Captions

Figure 1 Binary phase diagram of H_2+He mixtures to 75 GPa, signifying the phase transition of He-rich solid S_2 to S_3 at 52 GPa and a formation of metastable H_2-rich solid S_1' in He-rich mixtures. Closed (open) symbols with different colors denote compression (decompression) data for different He compositions as used for the rest of the figures. F, F_1, and F_2 refer respectively to homogenous H_2-He fluid mixture, H_2-rich fluid, and He-rich fluid, whereas S_1 and S_1' are H_2-rich solids and S_2 and S_3 refer to He-rich solids.

Figure 2 Raman spectral changes of H_2 vibrons in 1:1 H_2:He mixture along the 300 K isothermal compression to 75 GPa. F, F_1, F_2, S_1, and S_2 signify a homogeneous fluid mixture, H_2-rich fluid, He-rich fluid, H_2-rich solid, and He-rich solid, respectively, and their Raman spectra are plotted in different colors.

Figure 3 Raman spectral change of 1:1 H_2:He solid mixture at high pressures, plotted in the low frequency regions of (a) lattice phonon at 100-300 cm^{-1} and (b) H-He vibron at 2340-2440 cm^{-1}. (c) The H-He vibron at 20 GPa is also plotted as a function of He concentration, for comparison. The inset shows the peak intensity at 2370 cm^{-1}, normalized to that of the 2^{nd}-order diamond Raman at 2570 cm^{-1}, as a function of He concentration. The S_2 and S_3 signify He-rich solids at pressures below and above 52 GPa, respectively.

Figure 4 Pressure-dependent Raman shift of H_2 vibron in H_2+He mixtures at various concentrations below 12 GPa: (a, b) in the high-frequency region (a) below and (b) above 12 GPa, and (c) in the low-frequency region to 75 GPa. The inset in (a) represents a microphotograph of 1:9 H_2:He mixture at 12.6 GPa, showing coexistence of three different solid

phases, S_1, S_2 and S_1', and those of (b) and (c) refer to the H_2 vibrons of S_1' at 28 GPa of the same mixture.

Figure 1

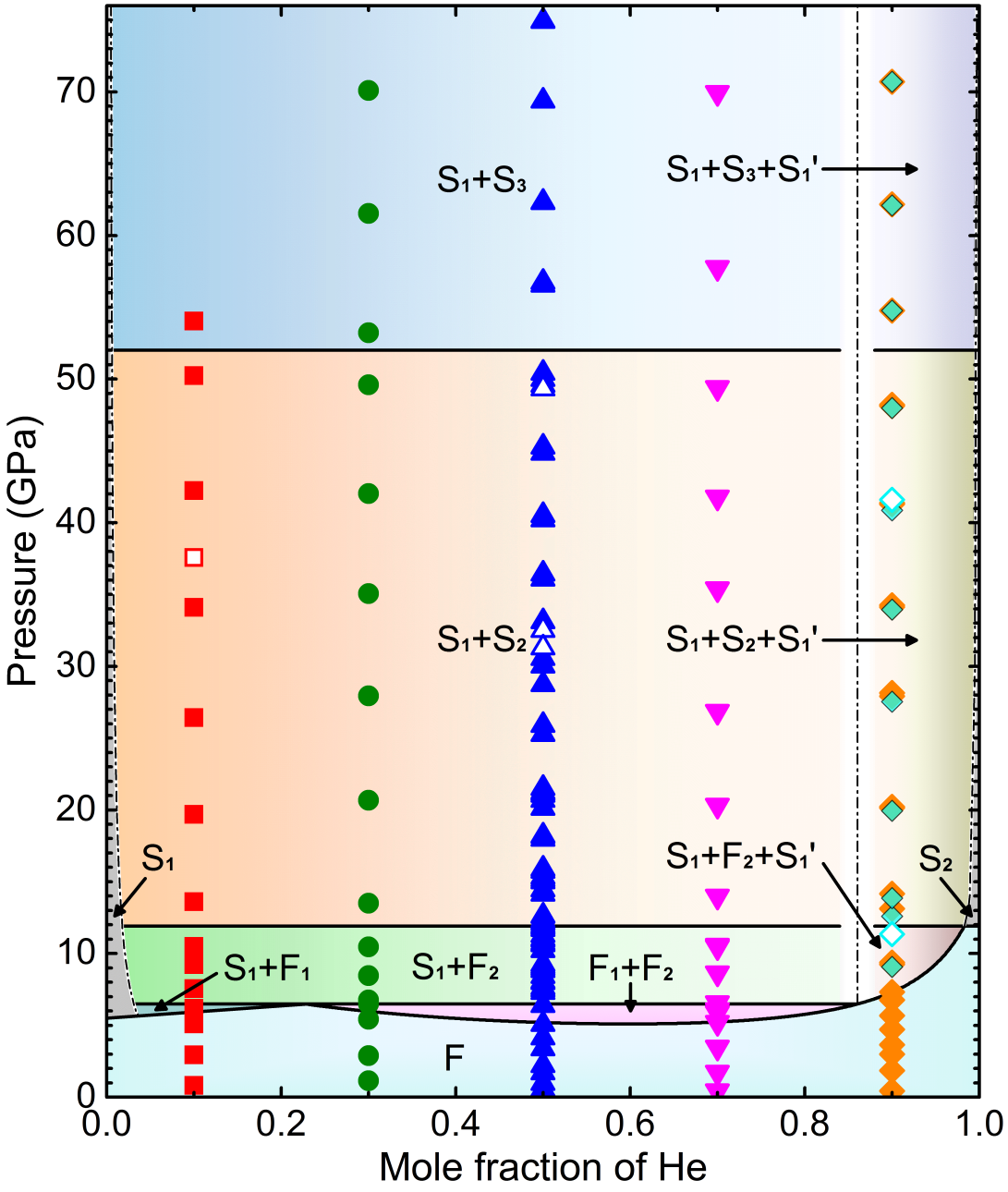
Pressure (GPa)
Mole fraction of He
0
10
20
30
40
50
60
70
0.0
0.2
0.4
0.6
0.8
1.0
S₁+S₃
S₁+S₃+S₁'
S₁+S₂
S₁+S₂+S₁'
S₁
S₁+F₂+S₁'
S₂
S₁+F₁
S₁+F₂
F₁+F₂
F

Figure 2

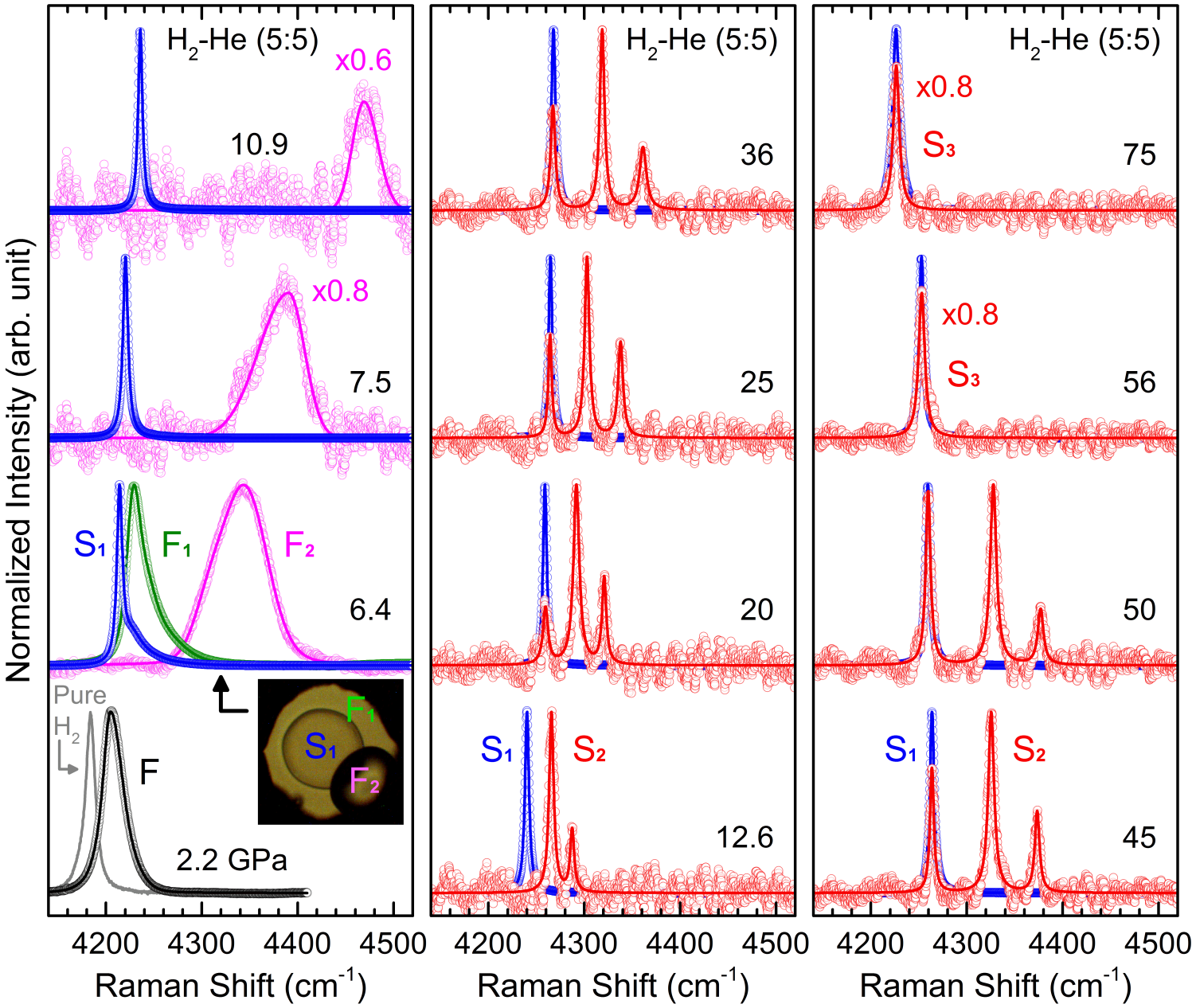
H2-He (5:5)
x0.6
10.9
x0.8
7.5
S1
F1
F2
6.4
Pure
H2
F
2.2 GPa
F1
S1
F2
H2-He (5:5)
36
25
20
S1
S2
12.6
H2-He (5:5)
x0.8
S3
75
x0.8
S3
56
50
S1
S2
45
Normalized Intensity (arb. unit)
4200
4300
4400
4500
Raman Shift (cm-1)
Raman Shift (cm-1)
Raman Shift (cm-1)

Figure 3

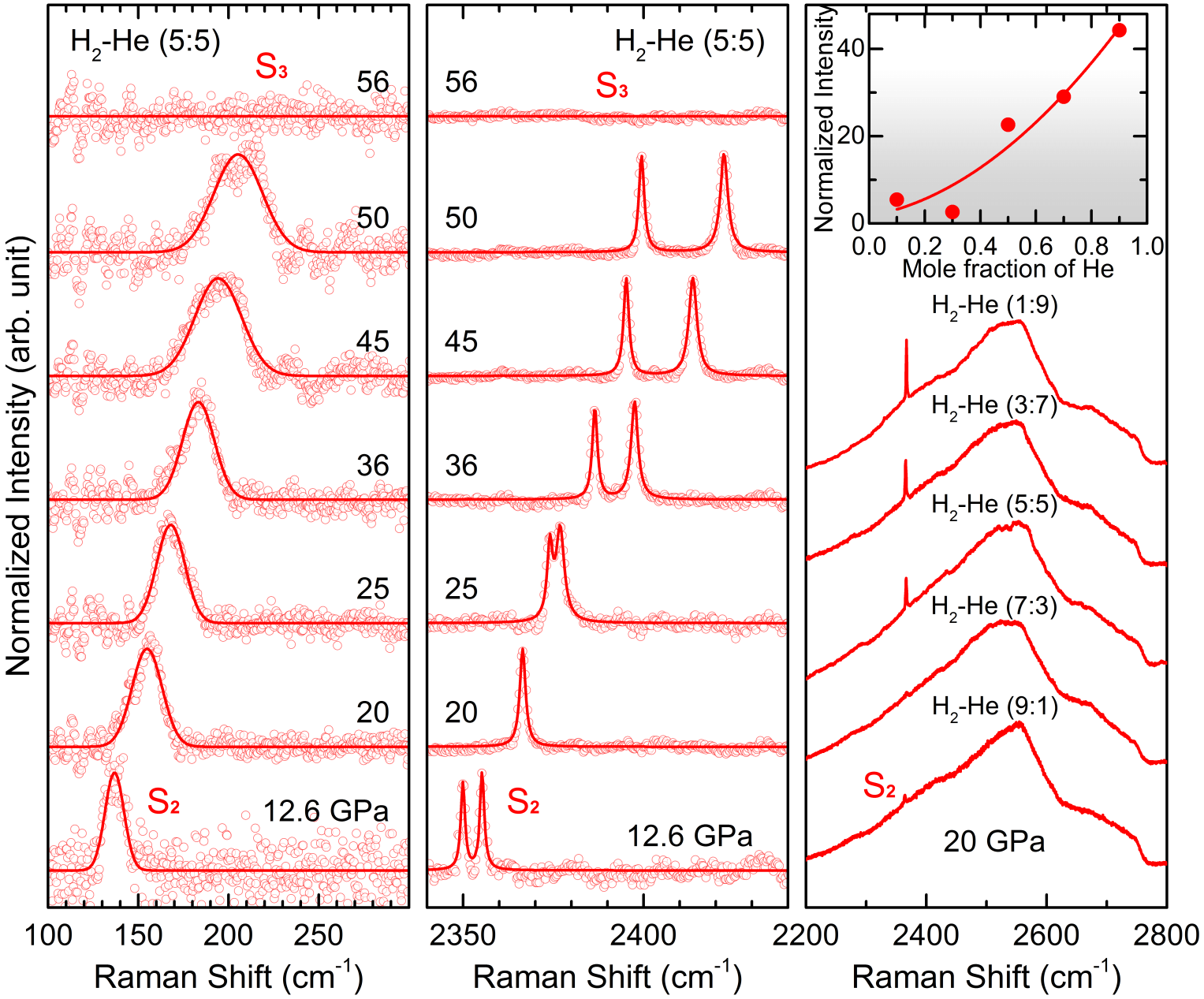
H2-He (5:5)
S3
56
50
45
36
25
20
S2
12.6 GPa
Normalized Intensity (arb. unit)
100
150
200
250
Raman Shift (cm-1)
2350
2400
Normalized Intensity
40
20
0
0.0
0.2
0.4
0.6
0.8
1.0
Mole fraction of He
H2-He (1:9)
H2-He (3:7)
H2-He (5:5)
H2-He (7:3)
H2-He (9:1)
20 GPa
2200
2400
2600
2800

Figure 4

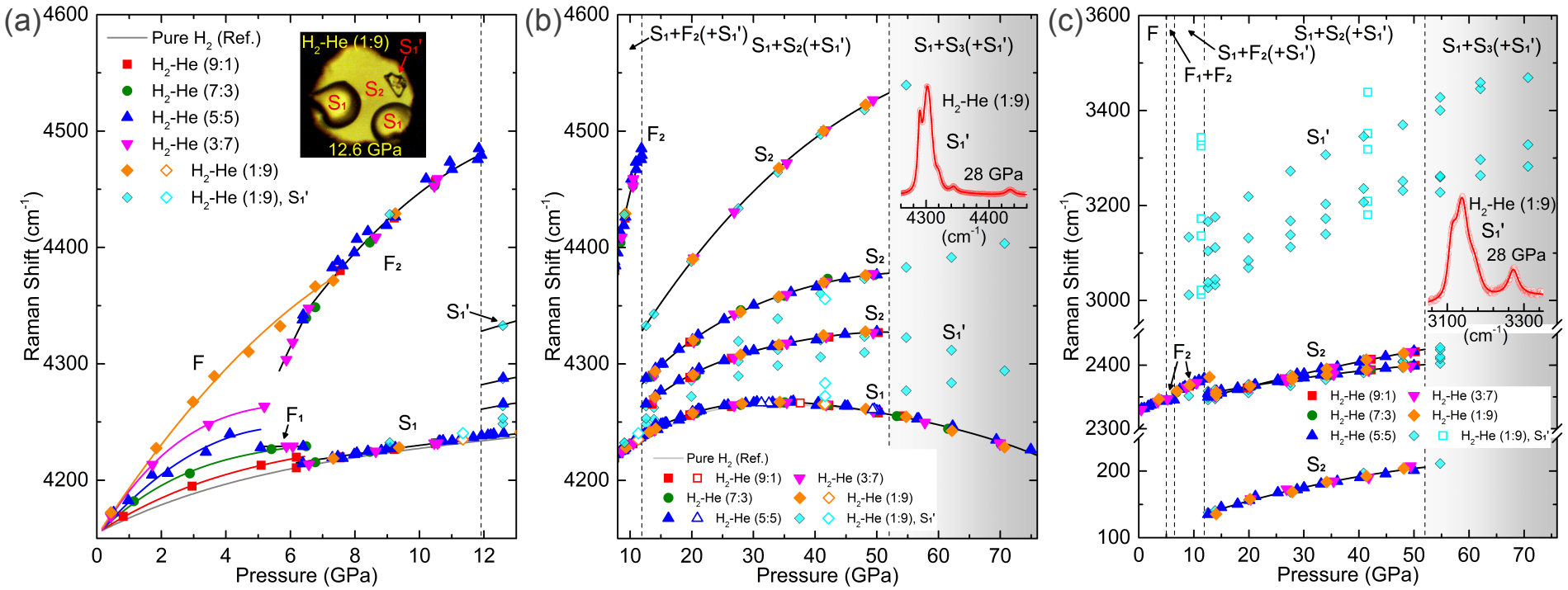
(a)
Pure H2 (Ref.)
H2-He (9:1)
H2-He (7:3)
H2-He (5:5)
H2-He (3:7)
H2-He (1:9)
H2-He (1:9), S1'
H2-He (1:9) S1'
S2
S1
S1
12.6 GPa
F
F1
F2
S1
S1'
Raman Shift (cm-1)
Pressure (GPa)
(b)
S1+F2(+S1')
S1+S2(+S1')
S1+S3(+S1')
F2
S2
S2
S1'
S1
H2-He (1:9)
S1'
28 GPa
4300 4400
(cm-1)
Pure H2 (Ref.)
H2-He (9:1)
H2-He (3:7)
H2-He (7:3)
H2-He (1:9)
H2-He (5:5)
H2-He (1:9), S1'
Raman Shift (cm-1)
Pressure (GPa)
(c)
F
F1+F2
S1+F2(+S1')
S1+S2(+S1')
S1+S3(+S1')
S1'
F2
S2
S2
H2-He (1:9)
S1'
28 GPa
3100 3300
(cm-1)
H2-He (9:1)
H2-He (3:7)
H2-He (7:3)
H2-He (1:9)
H2-He (5:5)
H2-He (1:9), S1'
Raman Shift (cm-1)
Pressure (GPa)